Interferometric 3D tracking of several particles in a scanning laser focus

Michael Speidel, Lars Friedrich, and Alexander Rohrbach

Laboratory for Bio- and Nano- Photonics, Department of Microsystems Engineering-IMTEK,
University of Freiburg, Georges Köhler Allee 102,79110 Freiburg,Germany
Corresponding author: rohrbach@imtek.de

Abstract: High-Speed tracking of several particles allows measuring dynamic long-range interactions relevant to biotechnology and colloidal physics. In this paper we extend the successful technique of 3D back-focal plane interferometry to oscillating laser beams and show that two or more particles can be trapped and tracked with a precision of a few nanometers in all three dimensions. The tracking rate of several kHz is only limited by the scan speed of the beam steering device. Several tests proof the linearity and orthogonality of our detection scheme, which is of interest to optical tweezing applications and various metrologies. As an example we show the position cross-correlations of three diffusing particles in a scanning line optical trap.

OCIS codes: (120.0120) Instrumentation, measurement, and metrology; (290.0290) Scattering; (140.7010) Trapping; (260.3160) Interference

References and links

1. D. Weihs, T. G. Mason, and M. A. Teitell, "Bio-Microrheology: A Frontier in Microrheology," Biophys. J. **91**, 4296-4305 (2006).
2. M. Brunner, J. Dobnikar, H. H. von Grunberg, and C. Bechinger, "Direct measurement of three-body interactions amongst charged colloids," Phys. Rev. Lett. **92**, 078301 (2004).
3. J. C. Crocker, J. A. Matteo, A. D. Dinsmore, and A. G. Yodh, "Entropic attraction and repulsion in binary colloids probed with a line optical tweezer," Phys. Rev. Lett. **82**, 4352-4355 (1999).
4. J.-C. Meiners and S. R. Quake, "Direct Measurement of Hydrodynamic Cross Correlations between Two Particles in an External Potential," Phys. Rev. Lett. **82**, 2211 (1999).
5. S. Henderson, S. Mitchell, and P. Bartlett, "Direct measurements of colloidal friction coefficients," Phys.Rev. E **64**, 061403 (2001).
6. M. Atakhorrami, K. M. Addas, and C. F. Schmidt, "Twin optical traps for two-particle cross-correlation measurements: Eliminating cross-talk," Rev. Sci. Instr. **79**, 043103 (2008).
7. M. Polin, Y. Roichman, and D. G. Grier, "Autocalibrated colloidal interaction measurements with extended optical traps," Phys.Rev. E **77**, 051401-051407 (2008).
8. G. Gibson, J. Leach, S. Keen, A. J. Wright, and M. J. Padgett, "Measuring the accuracy of particle position and force in optical tweezers using high-speed video microscopy," Opt. Express **16**, 14561-14570 (2008).
9. M. Speidel, A. Jonas, and E. L. Florin, "Three-dimensional tracking of fluoroscent nanoparticles with subnanometer precision by use of off-focus imaging," Opt. Lett. **28**, 69-71 (2003).
10. Z. Zhang and C.-H. Menq, "Three-dimensional particle tracking with subnanometer resolution using off-focus images," Appl. Opt. **47**, 2361-2370 (2008).
11. S.-H. Lee, Y. Roichman, G.-R. Yi, S.-H. Kim, S.-M. Yang, A. van Blaaderen, P. van Oostrum, and D. G. Grier, "Characterizing and tracking single colloidal particles with video holographic microscopy," Opt. Express **15**, 18275-18282 (2007).
12. L. P. Faucheux, G. Stolovitzky, and A. Libchaber, "Periodic Forcing of a Brownian Particle," Phys.Rev. E **51**, 5239-5250 (1995).
13. R. Verma, J. C. Crocker, T. C. Lubensky, and A. G. Yodh, "Entropic colloidal interactions in concentrated DNA solutions," Phys. Rev. Lett. **81**, 4004-4007 (1998).
14. J. Dobnikar, M. Brunner, H. H. von Grunberg, and C. Bechinger, "Three-body interactions in colloidal systems," Phys. Rev. E **69**, 031402 (2004).
15. F. Gittes and C. F. Schmidt, "Interference model for back-focal-plane displacement detection in optical tweezers," Opt. Lett. **23**, 7-9 (1998).
16. A. Rohrbach, C. Tischer, D. Neumayer, E. L. Florin, and E. H. K. Stelzer, "Trapping and tracking a local probe with a Photonic Force Microscope," Rev. Sci. Instrum. **75**, 2197-2210 (2004).

#104816 - $15.00 USD Received 2 Dec 2008; revised 12 Jan 2009; accepted 12 Jan 2009; published 13 Jan 2009

17. A. Pralle, M. Prummer, E.-L. Florin, E. H. K. Stelzer, and J. K. H. Hörber, "Three-dimensional position tracking for optical tweezers by forward scattered light," Microscopy Research and Techniques **44**, 378-386 (1999).
18. R. Nambiar and J. C. Meiners, "Fast position measurements with scanning line optical tweezers," Opt. Lett. **27**, 836-838 (2002).
19. D. Neumayer, P. Kaiser, E. H. K. Stelzer, and A. Rohrbach, "Interferometric tracking of two particles with dynamic optical traps," Proc. SPIE **5859**, 33-39 (2005).
20. A. Rohrbach, H. Kress, and E. H. K. Stelzer, "Three-dimensional tracking of small spheres in focused laser beams: influence of the detection angular aperture," Opt. Lett. **28**, 411 - 413 (2003).
21. J. K. Dreyer, K. Berg-Sorensen, and L. Oddershede, "Improved axial position detection in optical tweezers measurements," Appl. Opt. **43**, 1991-1995 (2004).
22. A. Rohrbach and E. H. K. Stelzer, "Three-dimensional position detection of optically trapped dielectric particles," J. Appl. Phys. **91**, 5474-5488 (2002).
23. J. Baumgartl, "Like-charge attraction in confinement: myth or truth?," Soft Matter, 631-635 (2006).
24. P. C. Seitz, E. H. K. Stelzer, and A. Rohrbach, "Interferometric tracking of optically trapped probes behind structured surfaces: a phase correction method," Appl. Opt. **45**, 7903-7915 (2006).

1. Introduction

In biotechnology and modern cellbiology a strong interest exists in the observation of intra cellular transport processes e.g. the diffusion and interaction of vesicles. Transport processes within a biological cell for example, depend on the hydrodynamic environment and changes in the viscosity close to walls, fibers and membranes. Thus bio-microrheology developed into an important research area [1] during recent years.

Optical tweezers serve as a useful tool to observe processes steered by Brownian motion and thus gained importance in microrheology and interaction measurements. A variety of new experiments became possible due to the tweezers' ability to trap and manipulate nanoscopic objects with optical forces.

In contrast to static interaction measurements [2, 3], experiments in the field of microrheology are often designed to measure dynamic interactions (e.g. hydrodynamic coupling) between two or several particles at high temporal resolution. It is therefore necessary to trap and track at least two particles at the same time. Common approaches are to use a line-trap or a twin-trap. The latter consists of two separated, orthogonally polarized beams, each of which is focused to a single point trap [4, 5]. Due to the high NA trapping lens used for focusing, a cross-talk between both polarization directions is introduced and position measurements need to be corrected for these correlations [6]. A line trap can also be created from a hologram [7], where. particle positions are then analyzed by video tracking.

Although acquisition speed increased with modern CMOS cameras [8], temporal resolution and accuracy are still limited – for technical and physical reasons. Additionally video tracking is mainly limited to two dimensions and thus often requires squeezing particles between two interfaces to minimize axial particle movements or fluctuations [7]. Although, progress in 3D, single particle tracking has been reported [9, 10], these methods are less flexible since they require recording calibration curves for each particle type before measurements and subsequent 2D curve fitting. Likewise holographic video tracking requires intensive post-processing [11] and has not yet proven its precision when particles are very close to each other.

Another approach is to rapidly scan a laser focus along a line. This effectively creates an optical potential, which is very smooth in direction of the line scan, but steep in the other two dimensions [12-14]. The effective potential depth can be either controlled by locally varying the laser scan speed or by changing the local laser intensity. This technique has proven to be suitable for precise particle interaction measurements [2, 3]. However, slow video tracking limits applications to static interaction experiments.

Therefore a very fast and precise 3D tracking technique such as back focal plane (BFP) interferometry is required, which mainly has been used for static point traps [15-17]. First attempts to extent this tracking method to scanning line optical tweezers have been successfully realized in one [18] or two [19] dimensions. A dynamic measurement bandwidth of up to 40 kHz was achieved with accousto-optic beam deflectors [18]. In this article we

#104816 - $15.00 USD Received 2 Dec 2008; revised 12 Jan 2009; accepted 12 Jan 2009; published 13 Jan 2009

show, how BFP interferometry with oscillating lasers can be improved and extended to three dimensions, which enables more realistic studies of dynamic bio-molecular and colloidal interactions.

This paper is structured as follows: In section 2, the experimental setup is described. The third section describes signal generation and data processing. Section four shows position traces and histograms. How to characterize the detector responses is described in part 5, followed by a detailed analysis of reconstruction and detection errors in part 6. Finally section 7 concludes with the hydrodynamic coupling between three 970 nm sized silica spheres.

2. Experimental configuration

The experimental setup can roughly be divided into a manipulation unit consisting of a scanning line optical tweezers, and an inline interferometric tracking unit with two quadrant photodiodes (QPDs) (see Fig. 1). A more detailed description of the instrumental setup can be found in [16] for a single QPD. The beam from a 1 Watt Nd:YAG laser (λ=1064nm, IRCL-1000-1064-S, Crystal Laser, Reno, NV) is intensity modulated by an acousto-optic modulator (AOM, AA.MT.110/a1.IR, Pegasus Optics, Wallenhorst, Germany) and the first order beam is deflected by two galvanometric scanning mirrors (SM, M2, General Scanning Inc., Watertown, MA). About 3% of the first order laser power is deflected onto a reference diode (InGaAs PIN-QPD, G8370 ϕ=1mm, Hamamatsu Photonics, Japan) to stabilize the laser power by an electronic feedback (TEM Messtechnik GmbH, Großer Hillen 38, 30559 Hannover, Germany), not shown in Fig. 1. NIR corrected lenses (L1, L2) translate the rotation of the XY scanning mirrors together with a water immersion microscope objective lens (OL, UPLAPO60X/IR NA 1.2, Olympus, Japan) into a lateral shift of the focused trapping beam. Two beam expanders (2X and 4X, not shown), one placed directly behind the AOM and the other after the lenses L1 and L2, lead to a 150 % over-illumination of the BFP of the objective lens. The beam is then focused by the OL into an open chamber, consisting of a cover slip with a fluid solution on top. The maximum laser power reaching the fluid is approximately 150mW. A water immersion dipping lens (63X Achroplan, 0.9 water, 44069, Carl Zeiss, Germany) mounted opposite to the objective lens (OL), serves both as condenser for brightfield illumination and as detection lens (DL) for scattered and unscattered laser light.

The BFP of the detection lens is imaged onto two quadrant photodiodes (QPD1, QPD2, InGaAs PIN-QPD, G6849, Hamamatsu Photonics, Japan) with different magnifications, by the lenses L3-L5. Over-illumination of one QPD increases both sensitivity and linear detection range for particle z-displacements [20, 21]. A non- polarizing beam splitter (BS) deflects light of equal power to both QPD diodes, recording the interference pattern between unscattered and forward scattered light. The QPD signals are electronically amplified (Öffner, MSR-Technik, Plankstadt, Germany) with a 3dB cut-off frequency of 0.85 MHz. A specimen placed in the object plane can be moved accurately in xyz- direction with a piezo scan table (not shown, Tritor 102 cap, Piezosystem Jena, Germany). A minimum step size of 1.2 nm can be achieved in all three directions.

Typically, the scanning length of the laser focus is L = 10 µm in x-direction and can be swept with a frequency of currently up to R = 1 kHz. The shape of the trapping potential $V(x)$ within the sample, is only determined by the AOM transmission $A(x)$, when the laser focus, i.e. the point trap, is displaced by $x_{tr}(t)$ along a line at constant velocity $v_x(t) = 2 \cdot L \cdot R$. In our case we applied a saw-tooth shaped signal to the x-scanning mirror as shown in Fig. 1. Simultaneously the laser power $|E_i|^2$ is modulated by the AOM with a Gaussian shaped

#104816 - $15.00 USD Received 2 Dec 2008; revised 12 Jan 2009; accepted 12 Jan 2009; published 13 Jan 2009

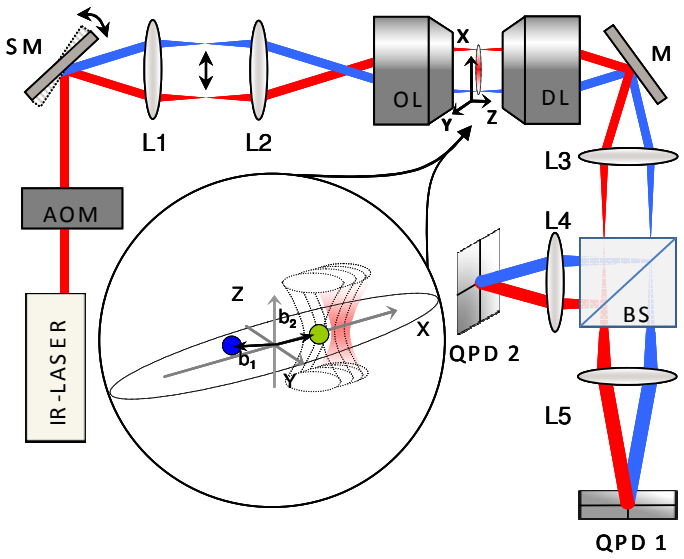

Fig. 1. (Color online) Schematic of the trapping and tracking setup. A NIR-laser is modulated by an AOM and deflected in phase by two galvanometric scan mirrors (SM). The rotational motion is translated into a lateral displacement by the scan lenses (L1, L2) and the objective lens (OL). The back focal plane of the detection lens (DL) is imaged onto two quadrant photodiodes for axial (QPD2) and lateral (QPD1) position detection. The inset shows a magnification of the focal plane, where the oscillating laser focus probes the positions $\mathbf{b}_1$ and $\mathbf{b}_2$ of two particles.

transmission function $A(x_{tr} = v_x \cdot t) \sim exp(-x_{tr}^2/\sigma^2)$ with maximum intensity $A(x_{tr}=0) \cdot |E_i|^2$ in the center of the line trap, corresponding to about 70mW. The width of the Gauss function $A(x_{tr})$ is about $2\sigma = 4\mu m$. The transmitted intensity $A(\pm x_{tr,max}) \cdot |E_i|^2$ is nearly zero at the turning points $\pm x_{tr,max}$.

2.1 Sample preparation

We use an open chamber as the sample cell, consisting of a fully transparent cover slip of 150 µm thickness. 200µl of ultra pure H_2O together with 2µl of 1:1000 bead solution are added on top (SiO_2 with natural hydroxyl or silanol (Si-OH) surface groups, Bangs Laboratories, Inc., 9025 Technology Drive Fishers, IN 46038-2886). The nominal bead diameter is 970 nm with a standard deviation <10%, a refractive index of 1.37 and a density of 1.96g/cm^3. Experiments are performed at room temperature (23 °C).

3. Principles of position detection

Although we are still in the very desirable situation that probing and trapping beam are identical, the position detection of a particle in a scanning line trap is more complex than in a in a static point trap, where $A(x_{tr}) = const.$ and $x_{tr} = const.$.

3.1 Signal generation

The interference intensity $I(k_x,k_y,\boldsymbol{b})$ between scattered and unscattered light is recorded with a QPD located in a conjugate plane of the detection lens BFP (coordiantes k_x and k_y). $\tilde{\mathbf{E}}_i(k_x,k_y,x_{tr})$ and $\tilde{\mathbf{E}}_s(k_x,k_y,x_{tr},\mathbf{b})$ denote the angular spectrum of the focused incident electric field and the field scattered at the diffusing particle at position $\mathbf{b}(t)$, relative to the trapping focus displaced by $x_{tr}(t)$. We assume a total interference intensity from the incident field $\tilde{\mathbf{E}}_i$ and the scattered field $\tilde{\mathbf{E}}_s(\mathbf{b})$,:

#104816 - $15.00 USD Received 2 Dec 2008; revised 12 Jan 2009; accepted 12 Jan 2009; published 13 Jan 2009

$$I(x_{tr},\mathbf{b}) = A(x_{tr})\cdot|\,\tilde{\mathbf{E}}_i(x_{tr}) + \tilde{\mathbf{E}}_s(x_{tr},\mathbf{b})|^2 \approx A(x_{tr})\cdot|\,\tilde{\mathbf{E}}_i(x_{tr})|^2 + A(x_{tr})\cdot|\,\tilde{\mathbf{E}}_s(x_{tr},\mathbf{b})|^2 +$$

$$A(x_{tr})\cdot 2\cdot|\tilde{\mathbf{E}}_i(x_{tr})||\tilde{\mathbf{E}}_s(x_{tr},\mathbf{b})|\cdot cos(\Delta\phi_x(b_x)+\Delta\phi_y(b_y)+\Delta\phi_z(b_z)) \qquad (1)$$

Here we further approximate that in the focal region a small displacement b_j of the particle results in a phase shift $\Delta\phi_j(b_j)$ only in this direction j (j = x,y,z) [16]. The Gouy-phase shift (also phase anomaly), inherent in divergent or convergent light, produces a phase shift $\Delta\phi_z(b_z)$ which is linear with the axial bead position b_z. At this stage, we further assume no interference between the scattered fields of N≥2 particles, which is reasonable when bead diameter D and focus width are the same.

The BFP-intensity in Eq. (1) generates the position signal $\mathbf{S}' = (S_x',\ S_y',\ S_z') = \mathbf{S}'(\mathbf{b},x_{tr})$, which changes with trap position $x_{tr}(t)$ and particle position $\mathbf{b}(t)$. As with the static trap, the position signal $S'(\mathbf{b}) = \int I(k_x,k_y,\mathbf{b})dk_xdk_y$ is obtained by integrating over the area A_m of the m-th PIN diode (m = 1..4):

$$S'_m\left(\mathbf{b}(t),x_{tr}(t)\right) \sim \iint_{A_m} A(x_{tr})\cdot\left|\tilde{\mathbf{E}}_i(k_x,k_y,x_{tr}) + \tilde{\mathbf{E}}_s(k_x,k_y,x_{tr},\mathbf{b})\right|^2 H(k_x,k_y)\,dk_x dk_y \qquad (2)$$

The PIN diode signals S'_m (m = 1…4) are all summed up to obtain the z-position signal $S_z'(\mathbf{b},x_{tr})$ and are connected such that the difference of a pair of adjacent diodes provides the lateral signals $S_x'(\mathbf{b},x_{tr})$ and $S_y'(\mathbf{b},x_{tr})$. The spatial filter function $H(k_x,k_y) = \theta(k_0\cdot NA_{det}\,f_A/f_B - (k_x^2+k_y^2)^{1/2})$ is defined by the magnification f_A/f_B of the numerical aperture NA_{det} of the detection lens, which is adjustable by the focal lengths f_4/f_3 and f_5/f_3. $\theta(k)$ is the Heavyside unit step function and cuts off the intensity in the BFP for larger radii.

The position signals $\mathbf{S}'(\mathbf{b},\ x_{tr}(t))$ along x form 3 time series $S_x'(t)$, $S_y'(t)$ *and* $S_z'(t)$, which must be further processed to obtain the final signals $\mathbf{S}(\mathbf{b}(t))$, which do not depend on x_{tr}. (note that these signals are without dash ′). Fig. 2 shows the $S_x'(t)$-signal (green line) as the superimposed detector responses of two particles and the axial response $S_z'(t)$ (blue line), which is additionally superimposed by the AOM modulated intensity $A(x_{tr})\cdot|\,\tilde{\mathbf{E}}_i(x_{tr})|^2$. The $S_x'(t)$-signal obtained from sweeping the laser across a particle is bipolar, due to the intensity

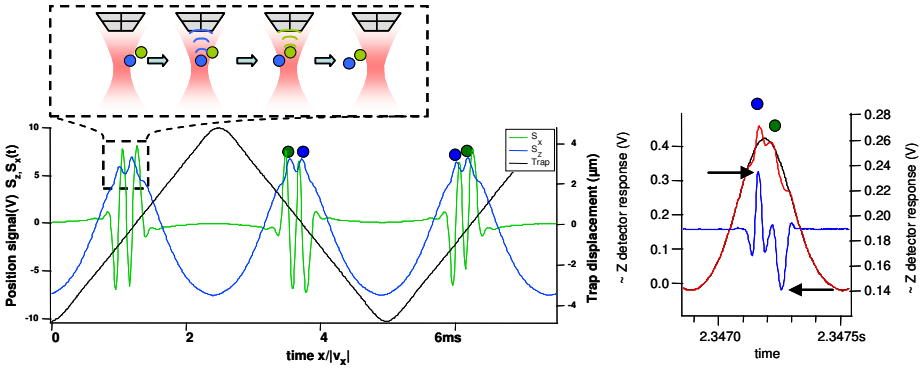

Fig. 2. (Color online) Time series $S_x'(t)$,and $S_z'(t)$ of the x (green) and z (blue) detector responses of two trapped particles. The trap positions x_{tr}(t) correspond to the black line. The axial sum signal is superimposed by the modulated laser intensity. Due to the back and forth motion of the trap, the positions (peaks) of each particle are horizontally flipped per scan. Right: z-raw data and "empty-scan" (red and black lines) and the resulting post processed z-data (blue) for two particles with z-positions, i.e. peak heights indicated by the arrows.

#104816 - $15.00 USD Received 2 Dec 2008; revised 12 Jan 2009; accepted 12 Jan 2009; published 13 Jan 2009

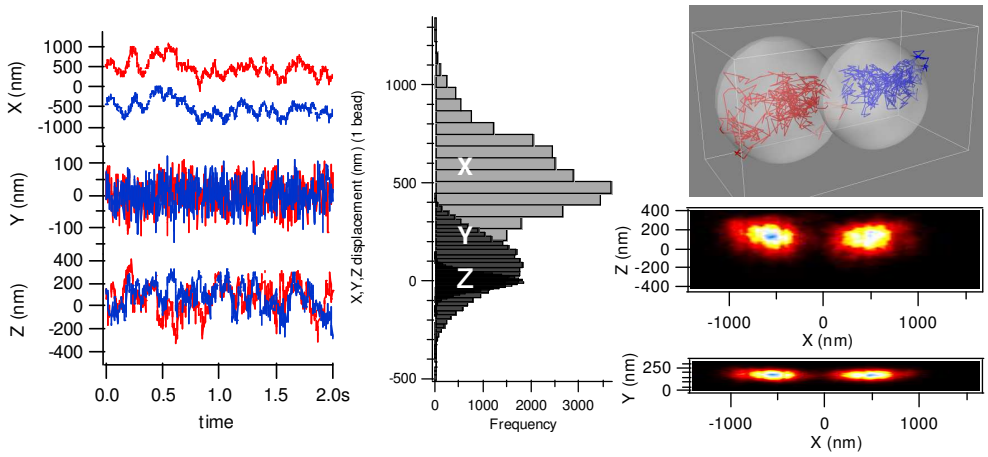

Fig. 3. (Color online) Left: time series of two 970 nm particles (red and blue traces) in a line trap. The distance between the x positions reveal the bead diameter. Center: Three 1D histograms of a single particle reflect the trap stiffnesses. Right: 2D histograms show how the particles distribute in the trap, which is also sketched above in 3D.

difference of two adjacent PIN diodes. One also has to consider, that due to the back and forth motion of the trap the positions of each particle are horizontally flipped between consecutive scans, as shown by the negative and positive slope of $x_{tr}(t)$ (black line).

3.2 Processing time series

We developed an algorithm which enables us to track two or more diffusing particles in the line tweezers, in three dimensions and with high accuracy.

The basic idea of the tracking algorithm is to differentiate the bipolar lateral time signal $S_x'(t)$, in order to obtain peaks at the corresponding particle centers. The temporally resolved lateral peaks are then converted to spatial positions b_x in nm according to $b_x(t) = 2 \cdot L \cdot R \cdot t$.

In other words, only the peak positions are relevant for the detection of the particle position b_x. The peak height, which is also modulated by the trapping intensity via the AOM does not influence the result. To increase precision, the $S_x'(t)$ peaks are fitted by a Gauss function before mapping them onto the mirror positions.

In contrast, the particle positions b_y and b_z are extracted only from the peak amplitudes. As shown in Eq. (1), these signals are superimposed by the overall intensity variation of the AOM, i.e. $A(x_{tr}) \cdot |\tilde{\mathbf{E}}_i(x_{tr})|^2$. To obtain the latter, a so called "empty-scan" $S_{es}'(t)$, *i.e.* without particles, is performed. In a first step during post processing the empty-scan is subtracted from the raw data according to:

$$S'\left(\mathbf{b}(t), x_{tr}(t)\right) - S'_{es}\left(x_{tr}(t)\right) \sim \iint_A A(x_{tr}) \cdot \left(\left| \tilde{\mathbf{E}}_i(x_{tr}) + \tilde{\mathbf{E}}_s(\boldsymbol{b} + x_{tr}(t)) \right|^2 - \left| \tilde{\mathbf{E}}_i(x_{tr}) \right|^2 \right) \cdot H \, dA \qquad (3)$$

The result of the operation in Eq. (3) is shown for the z-signal in Fig. 2 right. The axial positions b_z of both particles can be reproduced clearly from the peak heights. The peak height is proportional to the axial position b_z of the scatterer and only exists due to the Gouy phase shift. In a second step a Gauss function is fitted to each peak, in order to obtain an accurate measure of the peak height. Finally the fit parameters are divided by the corresponding AOM intensity, which is recorded by the reference diode. The same proceeding applies to the Y signal analysis. The extraction of the 3D position **b** can be summarized as follows:

#104816 - $15.00 USD Received 2 Dec 2008; revised 12 Jan 2009; accepted 12 Jan 2009; published 13 Jan 2009

$$
\begin{aligned}
b_x(t_0) &= x_{tr}(0) + v_x \cdot \mathrm{minpos}\left[\tfrac{d}{dt} S'_x(t)\right]_{t_0-\Delta t}^{t_0+\Delta t} \\
b_y(t_0) &= g_{yy}^{-1} \cdot \mathrm{extval}\left[S'_y(t)\right]_{t_0-\Delta t}^{t_0+\Delta t} \\
b_z(t_0) &= g_{zz}^{-1} \cdot \mathrm{extval}\left[S'_y(t) - S'_{es}(t)\right]_{t_0-\Delta t}^{t_0+\Delta t}
\end{aligned}
\tag{4}
$$

The time series are processed in the local time interval $2\Delta t < (2\cdot R)^{-1}$ around the particle position **b** at time t_0. g_{yy} and g_{zz} are detector calibration factors and are discussed in the next section. The function *extval* denotes the extremal value, the function *minpos* determines the position with the steepest slope of $S_x'(t)$, which is effectively the root of $S_x'(t)$, but avoids integrating a changing background intensity by taking the differential $^{d}/_{dt}$ instead.

4. Particle diffusion in an effective optical potential

Particles will diffuse in a time averaged optical potential which is mainly determined by optical gradient forces. Kicks from the passing trap should be negligible for sufficiently fast displacements at $v_x(t) = 2\cdot L\cdot R$. If we assume a intensity distribution in the focus $|E_i(x)|^2 = I(x) = I_0\cdot exp(-x^2/\Delta_x^2))$ in lateral direction, with a half focus width $\Delta_x = 0.61\cdot\lambda/NA$ defined by the *NA* of the trapping lens, the gradient force $F_{grad}(x)$ of a point trap can be approximated for small spheres with diameter $D << \lambda$ as

$$
F_{grad}(b_x) = \frac{\alpha n}{2cV} \int_{V(bead)} \nabla I(\mathbf{r} - b_x \cdot \mathbf{e}_x) dV \overset{D\ll\lambda}{\approx} \frac{\alpha n}{2c} \frac{\partial}{\partial b_x}\left(I_0 \cdot \exp\left(-\left(b_x / \Delta_x\right)^2\right)\right) \overset{b_x \ll \Delta x}{\approx} -\kappa_x \cdot b_x \tag{5}
$$

with polarizability α and speed of light c/n in medium with index n = 1.33. For small particle displacements b_x in the trap center, the linear approximation $F_{grad} = -\kappa_x\cdot b_x$ is justified. From Eq. (5) we find $\kappa_x \approx I_0\cdot\alpha\cdot n/(c\cdot\Delta_x^2)$ for the point trap at position x_{tr}. Also for the oscillating trap, one expects an effective three-dimensional optical trapping potential, $V_{eff}(\mathbf{b})$, which is elongated but harmonic in all three directions. The stiffnesses of $V_{eff}(\mathbf{b})$ are $\kappa_{x,eff}$, κ_y and κ_z such that $V_{eff}(b_x, b_y, b_z) = {}^1/_2\cdot(\kappa_{x,eff}\cdot b_x^2 + \kappa_y\cdot b_y^2 + \kappa_z\cdot b_z^2)$. Whereas κ_y and κ_z are mainly defined by the point trap and change only with the laser power $\sim A\cdot I_0$, the x-stiffness $\kappa_{x,eff} \sim (d^2/dx_{tr}^2)A(x_{tr})|_{xtr=0}$ can in addition be modified by the second derivative of the transmission function $A(x_{tr} = v_x\cdot t)$ at the point of maximum transmission $x_{tr} = 0$. The effective trapping potential along x can be averaged over a half scan period $(2R)^{-1}$ provided that $m/\gamma << (2R)^{-1}$ as follows:

$$
V_{eff}(b_x) = -\int_{-L/2}^{b_x} \left\langle F_{grad}(x,t) \right\rangle dx = -R \int_{-L/2}^{b_x} \int_{-(4R)^{-1}}^{(4R)^{-1}} A(v_x t)\cdot F_{grad}(x - v_x t)\, dt\, dx \overset{|b_x| \ll \frac{L}{2}}{\approx} \frac{1}{2}\cdot\kappa_{x,eff}\cdot b_x^2 \tag{6}
$$

Here $\gamma = 3\pi\cdot D\cdot\eta$ is the viscous Stokes drag and $\dot{x}$ the particle velocity. $V_{eff}(b_x)$ and the three trap stiffnesses can be obtained from the measured position histogram proportional to $p(b_x, b_y, b_z) = p_0\cdot exp\{-V(b_x, b_y, b_z)/kT\}$ as shown in Fig. 3 center. The vanishing AOM transmission $A(x=-L/2) = 0$ is the starting point for the integration of the effective force $\langle F_{grad}(b_x,t)\rangle$ to the potential $V_{eff}(b_x)$. The stiffness in x-direction is about 50fN/µm, about 2.5pN/µm in the y-direction and around 0.3pN/µm in the axial z-direction. These numbers refer to a single particle, which was tracked over 40 seconds and explored the whole trapping volume.

Experimental data of two particles diffusing in the line trap is shown in Fig. 3 left. The time series $b_x(t) \sim S_x(b_x)$ of the two particles (red and blue traces) are separated at minimum by the bead diameter of D = 970 nm. The 2D histograms on the right show the distribution of both particles within the optically created potential. This additionally gives an idea of the diffusive volume the particles explore. The trajectories are also shown in 3D with the particles indicated as scaled spheres.

#104816 - $15.00 USD Received 2 Dec 2008; revised 12 Jan 2009; accepted 12 Jan 2009; published 13 Jan 2009

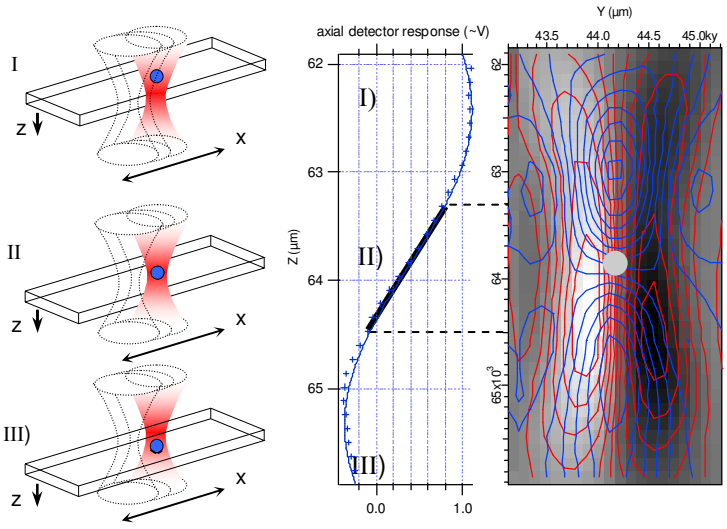

Fig. 4. (Color online) Linear detection range of the detector response of a 970nm silica sphere. Fixed on the coverslip, the particle is moved downwards in axial direction (see arrows) while the laser sweeps across it in x-direction. The method is illustrated for three different axial coverslip positions (I, II, III). The resulting detector response has a linear range (blue line) and the slope of a line fit encodes the axial sensitivity $g_z(b_z)$. A lateral movement of the coverslip results in the sensitivity $g_y(b_y)$. The contor plots for $g_y(b_y)$ and $g_z(b_z)$ are shown and the linear range is indicated by a black line.

For quantitative analysis, it is necessary to calibrate both, the optical trap and the detection system. In other words, the relation between optical forces **F**(**b**) and particle displacement **b** have to be determined, as well as the relation between detector responses S(**b**) and the particle displacement **b**. Therefore, we used the Langevin method described in detail in [16] under the assumption of a linear response such that $F_i(b_i) = \kappa_{ii} \cdot b_i$ and $S_i(b_i) = g_{ii} \cdot b_i$ where κ_{ii} and g_{ii} are diagonal matrices for the trap stiffness and the detector sensitivity, respectively ($i = x,y,z$). For a properly aligned optical system and well chosen spatial filters and lenses, this approximation is justified across the trapping volume. That means the contour lines of experimentally obtained detector responses S_x, S_y and S_z are orthogonal to each other. The experimental procedure for measuring the detector responses is sketched in Fig. 5.

5. Measuring the detection response

A particle is fixed on a coverslip due to an increased ion concentration (which enables binding of the bead to the coverslip by Van de Waals forces) and moved axially through the scanning focus. In addition, a lateral motion of the piezo in y-direction can be superimposed (meander scan). For known particle positions **b**, the signal response $S_y(0,b_y,b_z)$ and $S_z(0,b_y,b_z)$ can obtained alternatively to the Langevin method. However, the contour plots in Fig. 4 show in addition the quality of the tracking procedure. A line profile (blue line) through S_z, indicates the linear detection range (thick black line) and the slope corresponds to the sensitivity g_{ZZ}. Additionally the central trapping position of a particle is indicated in the contour plot (grey circle). This position appears to be in the center of the linear detection range. Within the linear region the contour lines of S_y and S_z intersect each other perpendicularly. This corresponds to a diagonal sensitivity matrix g_{ii}.

In the case of a line trap, the sensitivity matrix should remain constant over the extension of the scan range. As a control the described analysis of the detector sensitivity needs to be done at different positions in the trap. The resulting detector responses at three different positions (x_A, x_B, x_C) are given in Fig. 5. At positions x_B and x_C the fixed probe was placed

#104816 - $15.00 USD Received 2 Dec 2008; revised 12 Jan 2009; accepted 12 Jan 2009; published 13 Jan 2009

3µm away from position x_A, which corresponds to the trap center. Point x_A was determined by trapping a single particle in solution while approaching the surface of the coverslip slowly in axial direction, until the particle attached. Positions x_B and x_C are then reached by moving the piezo stage laterally. At each of the three positions (x_A, x_B, x_C) a data cube was recorded by moving the fixed particle in 110nm steps by the piezo actuator in z-axial and y-lateral direction through the scanning line trap. Fig. 5 shows the post processed detector responses S_x and S_z at the different positions after normalizing with the relative laser powers $A(x_A)$, $A(x_B)$, and $A(x_C)$. The slopes of each response at points x_A and x_C coincide relatively well with each other and do not show strong deviations. The signals $S_y(y)$ and $S_z(z)$ at position x_B have a slightly reduced sensitivity likely due to a non-optimal optical alignment, which however does not affect the overall tracking precision due to a small probability density at this position.

6. Position accuracy

Finally, to fully characterize the tracking method, several statistically independent sources of errors were considered, as there are: Electrical and mechanical noise, optical alignment and interference contrast and inaccuracies due to the sample rate used for data acquisition.

Mechanical stability and electrical noise are analyzed in Fig. 6(a). A particle fixed on a coverslip is moved by successive steps of the piezo actuator in axial (z) and lateral (x, y) direction. As a measure of precision, the standard deviation of the reconstructed steps $\sigma_i = g_{ii}^{-1} \cdot \sigma_{Si}$ is calculated (i = x, y, z). For better illustration the reconstructed particle positions are superimposed by a sliding average. Piezo driven steps of 10nm and 5 nm are easily resolved in x, y and z direction, respectively. A standard deviation of σ_x = 7.5 nm is assumed to be mainly due to the positioning noise of the galvanometric mirrors. A σ_y = 1.1 nm in y-direction is about that of a point trap. The z-precision (σ_z = 2.3 nm) is also close to that value.

Optical alignment and interference contrast: The position reconstruction, depending on the position of the particle in the trapping volume, was studied. For this purpose axial and lateral piezo steps b_j are compared with reconstructed steps S_j/g_{jj} in the linear range. The difference $\delta b_j = b_j - S_j/g_{jj}$ between the actual particle positions and the reconstructed positions is calculated and shown with histograms of position errors δb_x, δb_y and δb_z. in Fig. 6(b). In all three directions the distributions are slightly shifted towards positive errors, indicating that the displacements are underestimated by the detector. Similar findings were made for a point trap [22]. The (1/e) widths of the distributions are similar to those found for the mechanical instability and electronic noise.

Inaccuracies due to the sample rate: A systematic error is introduced in the reconstruction algorithm by the sample rate *f* of the data acquisition system. The number of sample points per lateral trap displacement is reduced at increased scan speeds v_{tr}. However, at some point the shape of the detector signal is influenced and the precision of the Gaussian fits will degrade. In order to quantitatively choose the proper rate, one data set of two diffusing particles was

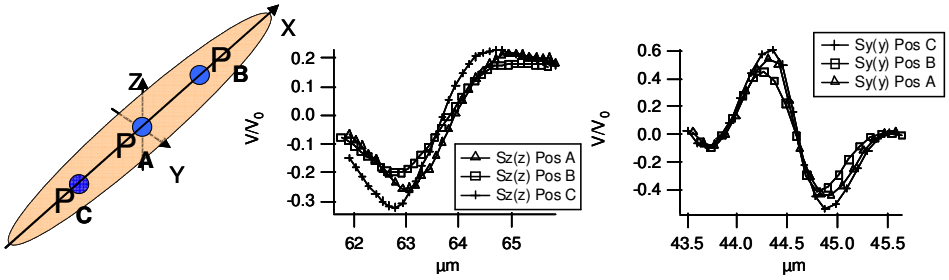

Fig. 5. (Color online) Detector responses S_y, S_z at the positions A, B and C within the optical potential. Points B and C are 3µm away from the center point A.

#104816 - $15.00 USD Received 2 Dec 2008; revised 12 Jan 2009; accepted 12 Jan 2009; published 13 Jan 2009

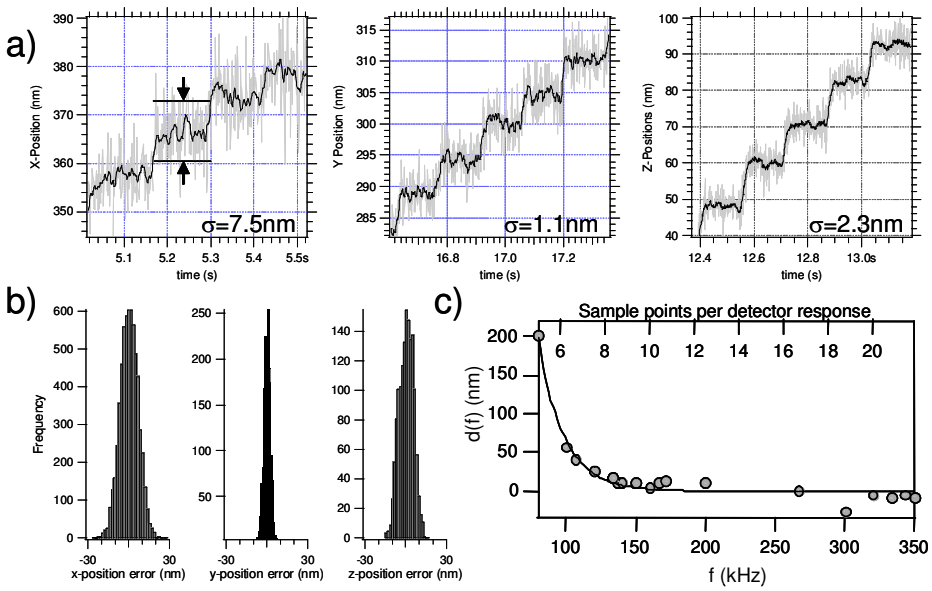

Fig. 6. Three different types of errors are summarized in the figures (a)-(c). In a) the influence of electronical and mechanical noise is characterized, b) describes optically induced errors and c) the influence of changes in the sample frequency.

analyzed by stepwise reducing the sample rate f. Afterwards the separation $\Delta b(f) = |\mathbf{b_1}-\mathbf{b_2}|$ between the particles was calculated from the reconstructed positions. The the result at maximum sample frequency f_{max} = 400 kHz was subtracted to obtain the error $d(f) = \Delta b(f) - \Delta b(f_{max})$. Fig. 6(c) shows the dependence of the distance error d on f. For sample rates smaller than f = 150 kHz d increases strongly due to imprecise Gaussian fitting. We therefore decided to record our data at a sample rate of f = 200 kHz. At higher sample rates f the error d still appears to scatter, mainly due to an inaccuracy in the z signal fit.

In particle video tracking difficulties arise, when the diffusing particles come in very close proximity to each other [23]. The tracking method introduced here is supposed to reliably track also adjacent or even slightly overlapping particles without significant cross talk in the reconstructed positions. To proof this robustness, two particles are tracked simultaneously with one being fixed on a coverslip, while the other diffusing freely in the optical potential. During tracking, the coverslip is step wise moved upwards, such that at some point the diffusing particle is also pushed upwards by the approaching coverslip. The reconstructed positions of the two particles are shown in Fig. 7(a). The axial 50 nm steps of the fixed particle are clearly resolved, and the reconstruction is almost independent on where the second particle is located. However a small influence becomes apparent when the spheres are in direct contact and both scattered fields E_{S1} and E_{S2} contribute to the interference at the QPD [24], such that Eq. (1) changes to

$$I(b_1,b_2) \sim |E_i + E_{S1}+E_{S2}|^2 \approx |E_i + E_{S1}|^2 + |E_i + E_{S2}|^2 + \mathrm{Re}\{E_{S1}\cdot E_{S2}^*\}. \quad (7)$$

Therefore, we investigated in a next step, how strongly the tracking precision in the x-direction was affected by an overlap Δx of two adjacent particles. The context is illustrated in Fig. 8(b). for two spheres with positions b_{x1} and $b_{x2}=(b_{x1}+D+\Delta x)$ Approximating that an x-position signal of two particles $|E_i + E_{S1}(b_{x1})+E_{S2}(b_{x2})|^2$ is a linear superposition of the responses of two individual particles $|E_i + E_{S1}(b_{x1})|^2$ and $|E_i + E_{S2}(b_{x2})|^2$ for a small crosstalk $\mathrm{Re}\{E_{S1}\cdot E_{S2}^*\}$ between the scattered fields, the following data processing procedure is

#104816 - $15.00 USD Received 2 Dec 2008; revised 12 Jan 2009; accepted 12 Jan 2009; published 13 Jan 2009

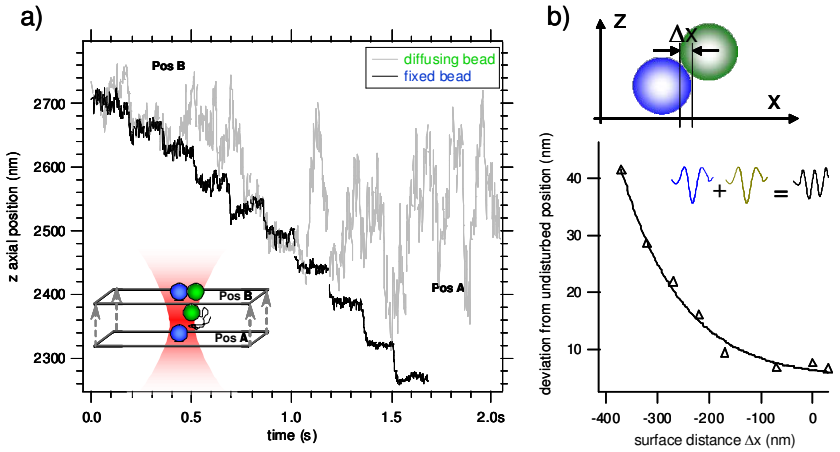

Fig. 7. (a). (Color online) The z-positions of two adjacent particles can be independently tracked. (b). Increase in the x-position reconstruction error as a function of the sphere overlap Δx between two particles (see text for details).

performed: Starting from zero overlap Δx = 0, two single particle detector response curves are superimposed with one bead diameter D apart and summed up to form the overall two particle signal. The tracking algorithm is then used to measure the distance between them. Comparing the measured distance with the simulated signal shift, defines a reconstruction error. Successively reducing the signal shift (decreasing Δx), results in the curve given in Fig. 7(b). An overlap of more than 100 nm in the x-lateral direction leads to an exponential increase in the reconstruction. However, we want to emphasize that these positions from imprecise signals occur only very rarely for line traps with trap stiffnesses as used in this paper.

7. Static and Dynamic interactions

From the histogram of the reconstructed particle positions the optical potential, probed by a diffusing particle, can be derived via Boltzmann statistics. The position histogram $H_{opt}(b_x) \sim p_{opt}(b_x)$ and the corresponding potential $V_{eff}(b_x) = -kT \cdot \ln(p_{opt}(b_x)) + V_0$ in laser scan direction (Eq. (6)) are shown in Fig. 8(a). A harmonic function fits well to the potential with a depth of almost 8 kT explored by the particle. Distance histograms of two particles diffusing in the potential $V_{eff}(\mathbf{b})$ are shown in Fig. 8(b). Here the two histograms $H(\Delta b)$ and $H(\Delta b_x)$ for the 3D distance $\Delta b = |\mathbf{b}_1 - \mathbf{b}_2|$ and the 1D distance $\Delta b_x = |b_{x1} - b_{x2}|$ of the two particles (bin size 20 nm) are compared. It is apparent that taking only Δb_x underestimates the center to center distance (mimimal $\Delta b_x < D$=970nm) and thus would lead to wrong interaction potentials $V(\Delta b)$, whereas taking the three-dimensional $\Delta b \geq D$ indicates the precision of our tracking method. The two particles appear to be most frequently separated by $\Delta b = D + 100$ nm.

As mentioned in the introduction, one aim of the developed tracking method is to analyze dynamic interactions between several diffusing spheres. The temporal resolution is defined by the number of points necessary to reliable sample the detector responses. Currently 12.5 points per µm are needed to identify a peak from a 970 nm sphere, which results in a temporal resolution of 2R = 1.6 kHz for the current setup. Substituting the galvanometric mirrors by acousto-optic deflectors would allow to increase the tracking rate up to 2R = 8 kHz, considering a signal amplifier bandwidth of approximately f = 1 MHz and a scanning length of L = 10 µm.

#104816 - $15.00 USD Received 2 Dec 2008; revised 12 Jan 2009; accepted 12 Jan 2009; published 13 Jan 2009

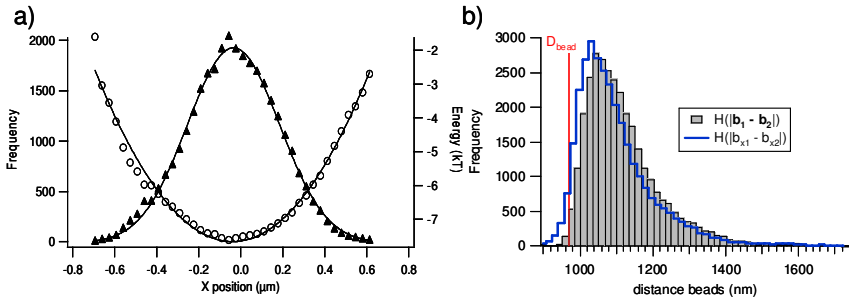

Fig. 8. (a). (Color online) Histogram of x-positions of a single particle and optical potential derived from Boltzmann statistics. (b). If two particles diffuse in the optical potential left, bead distances $\Delta b = |\mathbf{b}_1 - \mathbf{b}_2|$ vary. The histogram $H(\Delta b)$ of the 3D bead separation is compared to the histogram $H(\Delta b_x)$ calculated from the distances $\Delta b_x = |b_{x1} - b_{x2}|$ of lateral x- positions only. The bead diameter D is indicated by the red line (for details see text).

Another important aspect is the influence of the sweeping optical trap on the particle diffusion. Therefore we measured the kick-displacements Δ_{kick} in nm for various scan speeds of the laser trap. At a comparable laser power, the trap was moved in a circle, to enable kicking in only one direction. After some hundred passes of the trap the displacement due to laser trap kicking could be easily measured. The result is summarized in Table 1, where Δ_{kick} per kick decreases to about zero for trap speeds $v_{trap} > 30$mm/s. Such speeds can be easily achieved by AODs for line traps with extensions of L = 10µm.

As an application interesting to colloidal physics and nanoscopic particle transport we evaluated the cross correlation of the positions of three 970nm spheres in a scanning optical line trap. The cross- correlations shown in Fig. 9 reveal the hydrodynamic coupling between the spheres in a time window from 1/R = 1.25 ms to times limited by the AC-time of the trap in the corresponding direction. According to the different trap stiffness in the x, y and z direction, the interaction time can be measured over several 100 ms in the weak x-direction. In direction y and z, i.e. perpendicular to the scan direction, the correlation curves show a pronounced dip for neighbored particles (beads (12), beads (23)), but the anti-correlated motion is still visible for particles not being in direct contact to each other.

This anti-correlated behavior, known from two-particle interactions [4], is not observed in scan direction and likely is a result of laser trap kicking due to a too slow scan speed [12]. These inter-particle correlations will be discussed in more detail in a further paper, which is in preparation.

Table 1: Kick-displacements Δx_{kick} in nm for various speeds v_{trap} of the passing trap in mm/s.

v_{trap} (mm/s)	3	6	15	22	30	38	45
Δx_{kick} (nm)	63	13	4	2	0	0	0

8. Conclusions

In this paper we have discussed and explained in detail the principles of how to track several particles by back-focal plane interferometry using an oscillating laser beam. The system is in particular interesting to optical trapping applications, since trapping and tracking is achieved with the same beam and therefore does not require complicated alignment. Interferometric position signals are so pronounced that on the one hand tracking works very well even at low laser powers and low optical forces, and, on the other hand our tracking precision is less limited by photon shot noise than with high speed video-tracking. Video-methods including holographic techniques, have physical intrinsic problems concerning axial

#104816 - $15.00 USD Received 2 Dec 2008; revised 12 Jan 2009; accepted 12 Jan 2009; published 13 Jan 2009

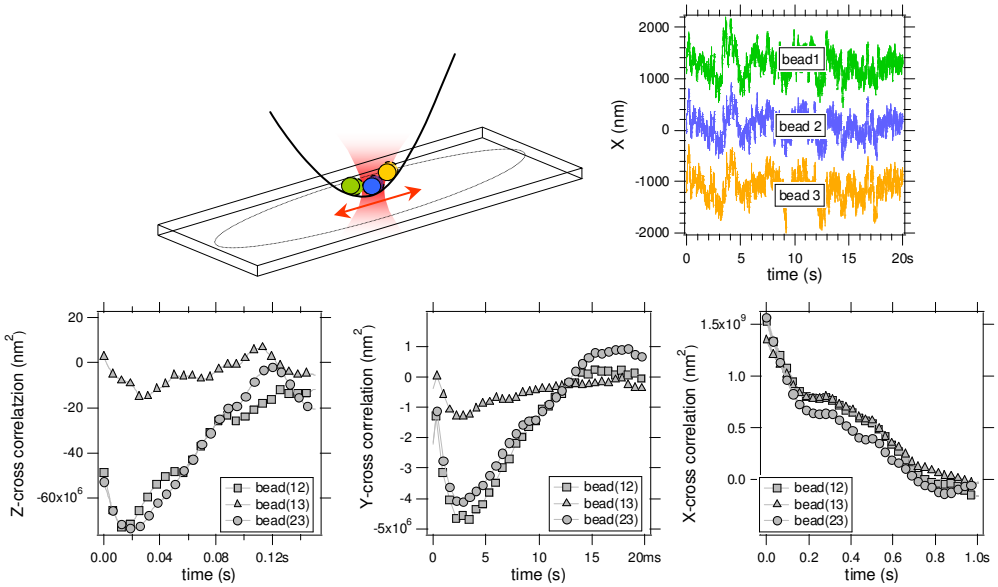

Fig. 9. (Color online) Cross correlation data of three 970nm particles in the line optical tweezers. The data reveal an anti-correlated motion due to hydrodynamic coupling between the particles in the y and z- direction, whereas the x-lateral direction shows a positively correlated motion. Cross talk between directly neighbored particles is pronounced compared to the outer most particles.

position tracking, especially for more than one particle, since out of focus intensity distributions must be know, which vary strongly with the degree of spatial and temporal coherence, with the angular spectrum of the incident light and with the particle properties. With our technique, tracking in 3D is possible without pre-calibration and at rates of several 10 kHz using AODs together with a fast signal sampling, which is offered nowadays by many medium cost DAQ cards.

Although in our approach particles have been tracked in scanning line tweezers, arbitrary scan curves different to a straight line can be programmed. Alike, the underlying optical potential can be modulated arbitrarily with an AOM or AOD, which does not affect our tracking precision or post-processing. The achieved tracking precision with the standard deviation of σ_x = 7.5 nm can be further reduced by a more stable scanning device, the very good σ_y = 1.1 nm in y- and σ_z = 2.3 nm in axial z-direction are superior to any other comparable tracking technique. The linear detection range is sufficiently large for trapping applications and can be further increased, by taking differently shaped laser foci for non-trapping applications. Since we used an oscillating point trap, we do not have problems with interference of scattered light (optical binding) as in static line traps, e.g. as with holographic optical tweezers.

We think that this study is helpful to a variety of optical tweezing labs, especially to those being aware of the great potential of dynamic particle interactions. Optical traps enable a diffusion and fluctuation driven interaction of binding partners with enhanced contact probability. The possibility to observe these motions in 3D, with nanometer precision and at high frame rates will open new doors in bio-technology and modern biology.

Acknowledgment

This work was supported by the Deutsche Forschungsgemeinschaft (DFG), grant number SP 1145. The authors thank Matthias Koch for reading the manuscript, as well as Dr. Christian Fleck and Fidel Córdoba Valdés for helpful discussions.

#104816 - $15.00 USD Received 2 Dec 2008; revised 12 Jan 2009; accepted 12 Jan 2009; published 13 Jan 2009